

Enhanced electron-electron correlations in nanometric SrRuO₃ epitaxial films

G. Herranz,* B. Martínez, and J. Fontcuberta

Institut de Ciència de Materials de Barcelona, CSIC, Campus UAB, Bellaterra 08193, Catalunya, Spain

F. Sánchez,† C. Ferrater, M. V. García-Cuenca, and M. Varela

Departament de Física Aplicada i Òptica, Universitat de Barcelona, Diagonal 647, Barcelona 08028, Catalunya, Spain

(Received 27 November 2002; published 29 May 2003)

Epitaxial and fully strained SrRuO₃ thin films have been grown on SrTiO₃(100). At initial stages the growth mode is three-dimensional- (3D-)like, leading to a finger-shaped structure aligned with the substrate steps and that eventually evolves into a 2D step-flow growth. We study the impact that the defect structure associated with this unique growth mode transition has on the electronic properties of the films. Detailed analysis of the transport properties of nanometric films reveals that microstructural disorder promotes a shortening of the carrier mean free path. Remarkably enough, at low temperatures, this results in a reinforcement of quantum corrections to the conductivity as predicted by recent models of disordered, strongly correlated electronic systems. This finding may provide a simple explanation for the commonly observed—in conducting oxides—resistivity minima at low temperature. Simultaneously, the ferromagnetic transition occurring at about 140 K, becomes broader as film thickness decreases down to nanometric range. The relevance of these results for the understanding of the electronic properties of disordered electronic systems and for the technological applications of SrRuO₃—and other ferromagnetic and metallic oxides—is stressed.

DOI: 10.1103/PhysRevB.67.174423

PACS number(s): 73.20.Fz, 73.63.Bd, 73.50.Gr

I. INTRODUCTION

The development of devices based on thin films is an active area of research. In particular, magnetic tunneling junctions with ferromagnetic oxide electrodes are interesting due to their promising technological applications. Successful fabrication of heterostructures requires to have a deep understanding of the effects related with the interfaces between layers. These effects may manifest itself in a variety of phenomena, including vacancies, structural disorder or phase segregation, and may be relevant to the transport and magnetic properties and thus, have a straightforward impact on the performance of the devices. Indeed, it has been recently demonstrated that the interface microstructure limits the spin-injection efficiency across heteroepitaxial interfaces in ZnMnSe/AlGaAs-GaAs spin-polarized light emitting diodes.¹ Manganite-based tunnel junctions such as La_{2/3}Sr_{1/3}MnO₃/SrTiO₃/La_{2/3}Sr_{1/3}MnO₃, also display a dramatic suppression of their performance at temperatures well below the Curie temperature. It has been proposed that this effect originates from complex electronic inhomogeneities existing at the interfaces of these heterostructures.² The extreme tendency of manganites towards electronic phase separation is intimately related to the double exchange mechanism of ferromagnetic coupling and the existence of strong electron-phonon coupling.

On the other hand, understanding of the impact of disorder in the electronic properties of strongly correlated systems is an important issue, since metallic oxides involving 3*d* or 4*d* metal transition ions are commonly used in heterostructures and, as will be shown below, microstructural disorder close to interfaces plays a major role.

In this paper we will focus on these important issues by exploring in detail the magnetotransport properties of epitaxial SrRuO₃ thin films as a function of thickness ($4\text{ nm} < t$

$< 320\text{ nm}$). SrRuO₃ is a promising material for using in technological applications.³ It is a metallic ferromagnet, whose ferromagnetism is tied to the conduction electrons lying in a π^* narrow band formed by the overlap of Ru t_{2g} orbitals with the O $2p$ orbitals.^{4,5} The itinerant character of magnetism in SrRuO₃ is well founded both theoretically and experimentally,⁴⁻⁶ and it has been proposed that the nature of the magnetic coupling in this compound should be more robust against interface effects when compared to double-exchange ferromagnets such as manganites.⁷ Small distortions induced in the lattice reverts in a narrowing of the π^* band that affect in a significant way its magnetic properties. In fact, substitution of Sr cations by other cations leads to the formation of non magnetic compounds such as CaRuO₃ or BaRuO₃, with crystalline structures differing slightly from that of SrRuO₃, due to slight tilts and rotations of the RuO₆ octahedra.⁸ This fact indicates that strain-induced effects arising from the film—substrate interactions could be relevant for the magnetotransport properties of SrRuO₃ films. On the other hand, the existence of strong electronic correlations in SrRuO₃ has been experimentally confirmed either from specific heat measurements,⁴ low-temperature transport behavior,⁹ or photoemission spectra,¹⁰ among others; it has also been found that the Fermi-liquid state is remarkably sensitive to disorder and breaks down at a very low temperature ($T \sim 10\text{ K}$), further confirming the significance of the electronic correlations.¹¹ Therefore, SrRuO₃ appears as an ideal candidate to explore the role of the growth-induced disorder on the transport properties of strongly correlated ferromagnetic oxides, a key issue in the field of spintronics.

Epitaxial thin films and heterostructures grown on a variety of substrates by different deposition techniques have been studied and their magnetic and transport properties analyzed.¹²⁻²³ In addition, there is some information about

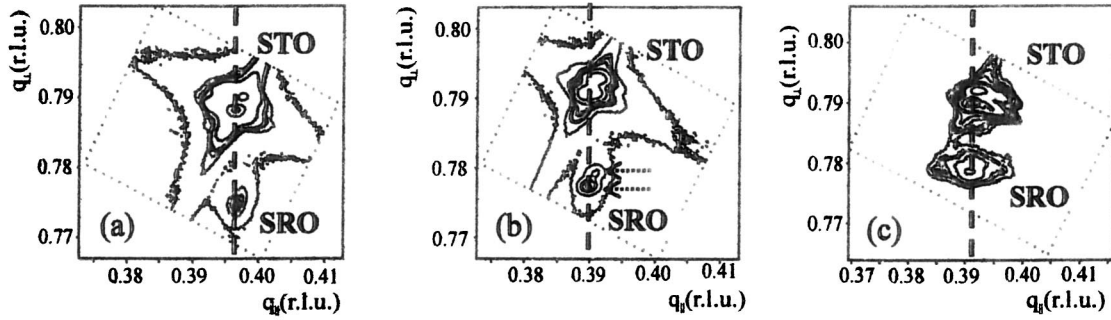


FIG. 1. Reciprocal space maps for different samples at the (204) reflection: (a) 40 nm, (b) 80 nm, (c) 320 nm. Arrows in (b) indicate the splitting of the peak due to $K_{\alpha 1}$ and $K_{\alpha 2}$ radiation.

the early stages of growth in SrRuO₃ films,^{14,21} but its correlation with physical properties is still lacking. The microstructure of films at nanometer scale, i.e., close to the interfaces, is closely related to the growth mechanism and may have a significant impact on the electronic properties of the film. Therefore it is necessary to undertake a thorough study on the thickness dependence of the magnetotransport properties in nanometric thin films. To the best of our knowledge, this study has only been performed on SrRuO₃/SrTiO₃ superlattices,^{12,13} but not in single films. In superlattices, a decrease of the Curie temperature was found as SrRuO₃ layer thickness decreases and this fact is attributed to a low-dimensional effect. Furthermore, the enhancement of the resistivity when reducing the SrRuO₃ layer thickness was attributed to scattering of conduction electrons at the SrRuO₃-SrTiO₃ interfaces.¹²

In this paper we report on structural and transport measurements for epitaxial SrRuO₃ thin films grown on SrTiO₃ (100) substrates. We will show below that the initial growth mode found in our films leads to a self-arranged pattern of defective regions that induces an in-plane anisotropy of the electrical transport. We present experimental procedures to reduce these defects and to control the density of the defective regions. We shall take advantage of the controlled presence of microstructurally disordered regions to study in detail the quantum corrections to the conductivity occurring at low temperature. We will show that this is intimately connected to the density of defects.

Finally, we will address the thickness dependence of the magnetic transition. We will show that the onset of ferromagnetism remains essentially constant down to $t \approx 6$ nm and thus is not determined by dimensional effects. However, the ferromagnetic transition becomes broader as the thickness of the films is reduced, likely as a result of microstructural defects originating from the film growth.

II. EXPERIMENTAL

SrRuO₃ thin films were grown on SrTiO₃(100) substrates by pulsed laser deposition with a KrF excimer laser ($\lambda = 248$ nm), with a pulse duration of 34 ns and a repetition rate of 10 Hz. The laser beam was focused to a fluence around 2 J/cm² and directed at an angle of 45° on a rotating target of stoichiometric SrRuO₃. The substrate was placed

parallel to the target at a distance of about 5 cm. The films were deposited at 750 °C and under an oxygen pressure of 0.1 mbar. When the laser was switched off, the oxygen pressure was slowly increased whereas the substrate was cooled down, reaching values of about tens of mbar during all the cooling. The films grown in this way will be labeled henceforth as series A films. No treatment of the substrates had been undertaken, prior to film deposition, to favor a particular atomic termination or to promote eventual surface reconstruction. However, atomic force microscopy (AFM) images revealed that as-received substrates, after heated to a temperature identical to that used for thin film deposition, display a clear miscut-originated terraces and steps topography.

Using these conditions a series of films of different thickness were prepared by changing the number of laser pulses.²³ The thickness (t) of the films, ranging from 4 to 320 nm, was measured by using either a stylus profilometer or x-ray reflectometry, and the structural quality and lattice parameters were investigated by using x-ray diffraction (XRD) measurements in a four-circle diffractometer using Cu K_{α} radiation. AFM working in tapping mode was used for surface characterization. Transport measurements were performed with the four-probe method, with contacts made on previously deposited Au, in a PPMS system (Quantum Design).

III. RESULTS I: MICROSTRUCTURE AND ELECTRICAL ANISOTROPY

Reciprocal space maps were performed for the (204) reflection. From these measurements, shown in Fig. 1, several conclusions can be drawn. First, all the films show an in-plane lattice parameter very close to the lattice constant of the substrate. Indeed, the data indicate that the in-plane lattice parameter of the films are $a_0 \approx 3.91$ Å, while the SrTiO₃ is a cubic perovskite with $a_0 = 3.905$ Å. It is remarkable that all films (4 nm $\leq t \leq 320$ nm) are found to be fully strained. Second, the out-of-plane lattice parameter is $c \approx 3.96$ Å for all the films, so the unit cell is slightly compressed in volume ($\sim 0.2\%$) with respect to the values of bulk SrRuO₃ (pseudocubic, $a_0 \approx 3.93$ Å). No significant variation of these lattice parameters with thickness is observed. Therefore, the SrRuO₃ unit cell of these films is always compressively strained in the plane of the film and undergoes a tensile stress in the out-of-plane direction. These data are similar to those

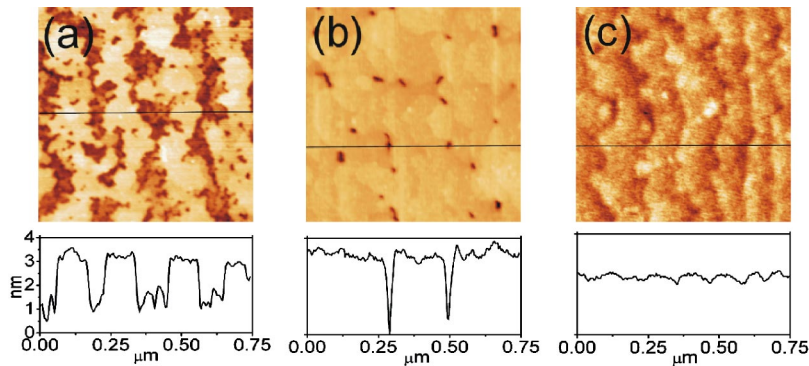


FIG. 2. (Color online) AFM surface images for films with (a) $t=4$ nm, (b) $t=8$ nm, and (c) $t=40$ nm.

reported by other authors, signalling a biaxial stress.¹⁵ On the other hand, the rocking curves, measured around the (002) reflection, are about $\Delta\omega=0.09^\circ$ wide (half-width at half maximum), irrespectively on the film thickness, demonstrating the good crystallinity of the films. This property can be also deduced from the shape of the reciprocal lattice peaks, in which the splitting due to $K_{\alpha 1}$ and $K_{\alpha 2}$ radiation is observable. Moreover, the ϕ scans, measured around the (022) reflection, indicate a good in-plane epitaxy.

The evolution of the surface morphology is summarized with the AFM images shown in Fig. 2. At early stages of growth [$t\approx 4$ nm, Fig. 2(a)] a fingerlike pattern formed by three-dimensional elongated islands following the [100] direction of the substrate is developed. At intermediate values of thickness [$t\approx 8$ nm, Fig. 2(b)] there is a coalescence of these islands. The islands are well connected, although a number of holes, with a maximum depth of ~ 5 nm, remain visible on the film surface. The most noticeable is that a structure of terraces starts to develop, and thicker films [Fig. 2(c)] show a well-defined structure of terraces and steps,

which typically have one unit-cell height. The terraces are smooth, and a very low roughness (root mean square value) of 0.13 nm is determined on a $1 \times 1 \mu\text{m}^2$ image. The terraces have the same direction and width that those observed (not shown) on the substrates (miscut angle $< 0.2^\circ$). This fact, and the low number of two-dimensional islands, suggests that the growth mode is step flow. The observed transition from a 3D to a 2D growth mode is surprising, and it will be described elsewhere.²⁴

This remarkable transition, whereby a 2D step flow occurs at thickness around 10 nm subsequent to a 3D finger-patterned growth at first stages, might have some consequences on the transport properties of the specimens. Indeed, a striking effect is observed in the resistivity. Electrical currents were injected in two orthogonal directions, and the respective measured resistivities are designated as ρ_{\parallel} and ρ_{\perp} . These directions were chosen so that they were aligned along and normal to a [100] direction of the substrate. As illustrated in Figs. 3(a)–3(c) the resistivity displays the typical metallic behavior of SrRuO₃. For the thickest film

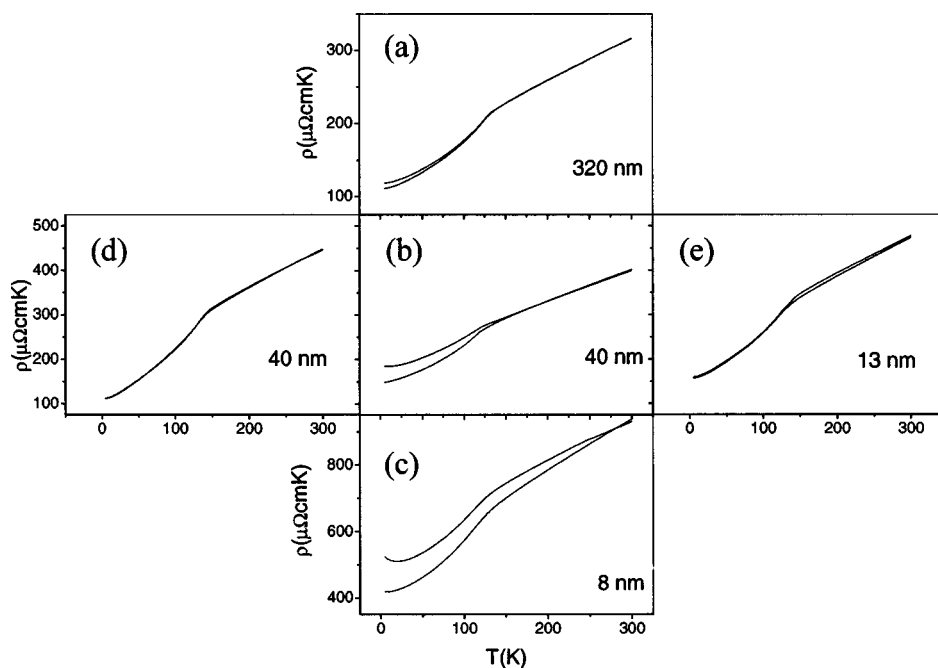


FIG. 3. Plot of the ρ_{\perp} - T and ρ_{\parallel} - T curves for three films of series A [(a) $t=320$ nm, (b) $t=40$ nm, (c) $t=8$ nm], showing the in-plane transport anisotropy. On the contrary, in films of series B either cooled in Ar (d) or in O₂ (e) this anisotropy vanishes.

($t \approx 320$ nm) we measured $\rho(300\text{ K}) \approx 240\ \mu\Omega\text{ cm}$, similar to previously reported values for epitaxial films and single crystals. Due to the peculiar growth mechanism, the thickness of the thinner films is not well defined. In spite of this, nominal values, determined from the number of laser pulses, have been used to compute the resistivities and these values are used throughout.

From the measurements plotted in Figs. 3(a)–3(c) one can conclude that (i) at any temperature, ρ increases when reducing the thickness and (ii) a clear anisotropy is observed, with $\rho_{\parallel} < \rho_{\perp}$ which reduces when increasing the film thickness. In the light of the peculiar growth mechanism occurring in these films, it is reasonable to correlate ρ_{\parallel} with current injection along the [100]-aligned finger-shaped 3D islands observed in the AFM images, whereas ρ_{\perp} corresponds to current that is essentially perpendicular to them. One must draw attention to the fact that the $t=40$ nm film [Fig. 3(c)] still shows a prominent in-plane resistivity anisotropy, in spite of having a very regular surface morphology.

The experimental data coming from the AFM images combined with the observed ($\rho_{\parallel}, \rho_{\perp}$) anisotropy, convincingly suggest that a well patterned structural and a concomitant electronic disorder appear in films of series A. The fact that the anisotropy progressively is wiped out as the thickness is increased indicates that this disorder is more prominent near the film-substrate interface. This is not surprising, if one considers the growth mechanism just discussed.

Before reaching the 2D growth, there is coalescence of the finger-shaped islands. At the edges where these grains merge together there could be some oxygen content depletion as a part of microstructural disorder that could allow some strain relief. With the aim of checking whether our films were oxygen deficient, we prepared films grown in the same conditions as those of series A, but once the growth had finished, the samples were cooled down to room temperature in an oxygen rich atmosphere, by introducing a pressure of 1 bar inside the chamber at a temperature of 530 °C. Note that in this way we also changed the cooling rate with respect to films of series A. These films are labeled hereafter as films of series B. X-ray diffraction data showed no difference in the structural parameters with respect to films of series A.

The *in situ* annealing described above for films of series B resulted in a suppression of the ($\rho_{\parallel}, \rho_{\perp}$) anisotropy, as is seen in Fig. 3(e). With the purpose of exploring further and eventually confirming whether the remarkable features appearing in the transport properties of films of series A could be attributed to a lack of oxygen at the grain boundaries, we performed some *ex situ* annealings in oxygen ($P_{\text{O}_2} = 1$ bar, 45 min, 500 °C) on series A films, reproducing similar conditions found in the *in situ* annealing of films of series B. However, attempts to oxygenate the films of series A were unsuccessful since the anisotropy of the transport properties remained. Consequently, we conclude that the in-plane transport anisotropy is closely related to microstructurally disordered, but likely well-oxygenated regions, formed at grain boundaries.

It has been recently observed, by using x-ray synchrotron radiation²⁵ that SrRuO₃ undergoes a series of phase transfor-

mations (polymorphism), going from an orthorhombic *Pnma* structure at room temperature, changing continuously to *Imma* at about 685 K, then changing discontinuously to tetragonal *I4/mcm* at about 825 K, and finally, changing continuously to a cubic structure at 950 K. This result provides a very simple and natural way to rationalize the present experimental observation. The different phases of SrRuO₃ differ essentially in the tilt of the RuO₆ octahedra and, therefore, on the Ru 4*d*–O 2*p* bandwidth and then on their transport properties. The residual stress at the grain boundaries may promote the local presence of some particular phase of the polymorphic family, which certainly are unobservable by conventional x-ray diffraction, and the electrical transport around and close the step edges may be rather different. As the tetragonal to orthorhombic transition is a first order one,²⁵ the cooling rate should be very relevant to determine its relative concentration. With the purpose of having a deeper insight in the possible role of the cooling rate, we performed an additional experiment preparing a film of series B, but substituting oxygen by argon; namely, once the growth had finished, an argon pressure of 1 bar was introduced inside the chamber at a temperature of 530 °C. Thus, we keep a similar cooling rate than in series B but in an oxygen-free atmosphere. As shown in Fig. 3(d), this annealing lead to films with no anisotropy at all, thus supporting the view according to which the cooling rate has a key role in the observed anisotropic behavior. This argument illustrates that the existence of the complex phase transformation in SrRuO₃ upon cooling has a profound impact on the transport properties.

The observed microstructural disorder has important consequences on the magnetotransport properties: on one hand, there is a conductivity depression at the lowest temperature signalled by the appearance of minima in the resistivity and,

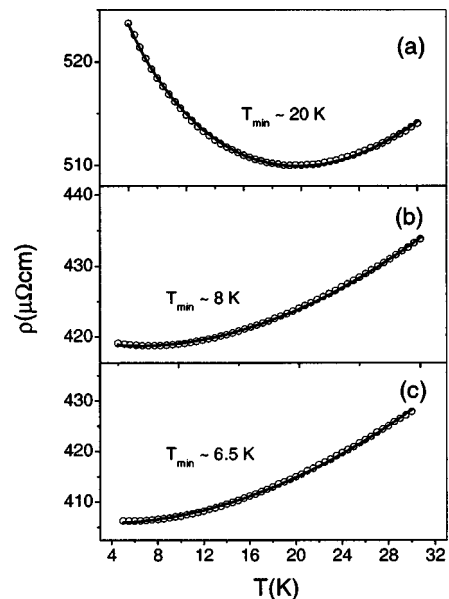


FIG. 4. The low-temperature ($5\text{ K} \leq T \leq 30\text{ K}$) resistivity is plotted for the films: (a) 8 nm series A (ρ_{\perp}), (b) 8 nm series A (ρ_{\parallel}), and (c) 6 nm series B. The temperatures at which the minima appear are indicated, as well as the fittings to the expression (3) (solid lines).

on the other hand, the ferromagnetic transition becomes broader. Both effects are enhanced as disorder increases. In the following we will discuss in detail both issues.

IV. RESULTS II: LOW-TEMPERATURE ELECTRICAL TRANSPORT

With the aim of determining the effect of microstructural disorder on the electronic properties, we take advantage of the controlled presence of defective regions by using the low-temperature transport data in the thinner films. We use the data collected for the $t=8$ nm of series A (both ρ_{\parallel} and ρ_{\perp}) and those of ρ_{\parallel} of the $t=6$ nm film of series B. Detailed inspection of the low-temperature region of the resistivity-temperature curves reveals the existence of minima in resistivity appearing at $T \leq 20$ K. In Fig. 4 the temperature dependence of the resistivity is plotted for the film 8 nm thick (series A) for both ρ_{\parallel} and ρ_{\perp} (inset) and for the film 6 nm thick (series B). The temperatures at which the minima appear are also indicated. Note that ρ_{\perp} of the 8 nm film shows a minimum at about 20 K, whereas for ρ_{\parallel} the minimum is at about 8 K, and for the 6 nm film it is at 6.5 K. This means that disorder is more prominent in the first case, while for the two latter it is weaker. One can discard the Kondo effect, associated with the scattering of the conduction electrons by isolated localized magnetic impurities as a possible source for the formation of the resistivity minima. Indeed the formation of localized magnetic moments in SrRuO₃ is not likely to occur, as it is a metallic itinerant ferromagnet whose magnetism is tied to the conduction electrons lying in a narrow π^* band. The narrowing of this conduction band, that is attained, for instance, by inducing distortions in the crystal-line structure by substitution of Sr cations by other cations, leads to the formation of nonmagnetic compounds, such as CaRuO₃ or BaRuO₃.²⁶ On the other hand, as observed in Fig. 5 for the film with $t=8$ nm (series A), the application of a field of 5 T induces only a small magnetoresistance but does not remove the minima signalling its nonmagnetic origin. Therefore, in agreement with López de la Torre *et al.*,⁹ we conclude that the Kondo effect is not likely to be the source of the low-temperature ρ minima commonly observed in SrRuO₃ thin films.²⁷ An alternative nonmagnetic mechanism leading to resistivity minima could be disorder induced localization, either through weak localization or by electro-electron enhanced interactions.²⁸⁻³⁰ In order to elucidate the possible relevance of these mechanisms, we have done a careful analysis of the temperature dependence of the low-temperature resistivity.

Following Altshuser and Aronov²⁹ and Abrikosov,³⁰ we

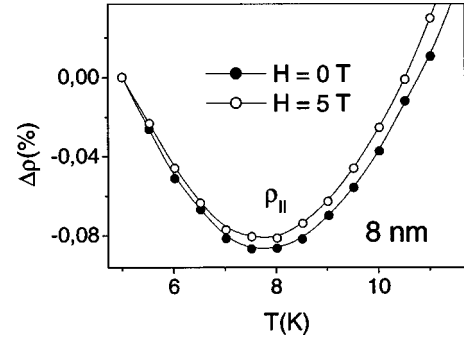


FIG. 5. Plot showing $\Delta\rho_{\parallel} = (\rho_{\parallel} - \rho_{\parallel 5K}) / \rho_{\parallel 5K}$ for the film with $t=8$ nm (series A) in zero field and under an applied field of 5 T.

consider a model including quantum corrections to the conductivity in 3D systems. Within this framework, the low-temperature dependence of the conductivity can be described by

$$\sigma(T) = \sigma_0 + aT^{1/2}, \quad (1)$$

where the first term is the usual temperature independent elastic scattering from defects, and the second is related to quantum corrections from e^-e^- interactions. As shown by Abrikosov, these corrections can be estimated by using the expression³⁰

$$\frac{\sigma - \sigma_0}{\sigma_0} \sim \left(\frac{\lambda_F}{l} \right)^{3/2} \left(\frac{k_B T}{\mu} \right)^{1/2}, \quad (2)$$

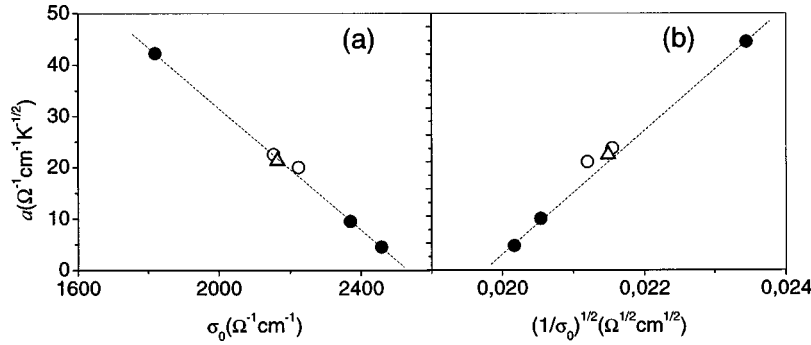
where $\mu \approx E_F$ (the Fermi energy), λ_F is the electronic Fermi wavelength, and l is the mean free path. Knowing that $E_F \approx 2$ eV, $m^* \approx 3.7m_e$ (see Ref. 4), we can estimate $\lambda_F \approx 4.5$ Å. The mean free path l is estimated from $\sigma = ne^2\tau/m^* = ne^2l\lambda_F/h$, with $n \approx 2 \times 10^{22}$ cm⁻³ (Ref. 20). For our samples, $\sigma \approx 2 \times 10^3$ Ω⁻¹cm⁻¹ at 5 K, so the mean free path is $l \approx 5-6$ Å at low temperature, so we have $k_F l \approx (2\pi/\lambda_F)l \approx O(1)$ in our films. Therefore, we expect the quantum corrections to the conductivity given by Eq. (2), to be relevant at low temperature.

Assuming that the Mathiessen's rule holds, and in order to account for higher order scattering mechanisms and to extend analytical description to higher temperatures, an additional T^2 term should be included. Accordingly the resistivity data has been fitted to

$$\rho = \frac{1}{\sigma_0 + aT^{1/2} + bT^2}. \quad (3)$$

TABLE I. Results of fittings to the expression $\rho = [1/(\sigma_0 + aT^{1/2})] + bT^2$ in the range $5 \text{ K} \leq T \leq 30 \text{ K}$ for a thin film of series A with $t=8$ nm (fittings corresponding to σ_{\perp} and σ_{\parallel}) and for a thin film of series B with $t=6$ nm. The temperatures at which the ρ - T curves reach a minimum (T_{\min}) are also indicated.

	σ_0 (Ω ⁻¹ cm ⁻¹)	a (Ω ⁻¹ cm ⁻¹ K ^{-1/2})	b (ΩcmK ⁻²)	T_{\min} (K)
8 nm (ρ_{\perp})	1819 ± 1.0	42.2 ± 0.3	2.96 × 10 ⁻⁸ ± 3 × 10 ⁻¹⁰	20 K
8 nm (ρ_{\parallel})	2370 ± 1.0	9.6 ± 0.3	2.30 × 10 ⁻⁸ ± 2 × 10 ⁻¹⁰	8 K
6 nm	2458 ± 1.0	4.5 ± 0.5	2.80 × 10 ⁻⁸ ± 3 × 10 ⁻¹⁰	6.5 K



As evidenced by the solid lines through the experimental data, Eq. (3) allows obtaining excellent fits of $\rho(T)$ in a wide ($5 \text{ K} \leq T \leq 30 \text{ K}$) temperature range (Fig. 4). The results of our fits are summarized in Table I. The T^2 term in Eq. (3), is usually ascribed to electron-electron scattering taking into account Pauli's exclusion principle. The b coefficient can be evaluated by using³⁰

$$b \sim \frac{m^* k_B^2}{ne^2 \hbar E_F}. \quad (4)$$

From this expression we estimate $b \approx 4 \times 10^{-12} \Omega \text{ cm K}^{-2}$, that is 3–4 orders of magnitude smaller than our measured value ($b \approx 2-3 \times 10^{-8} \Omega \text{ cm K}^{-2}$). This important discrepancy was already noted by Klein *et al.*²⁰ (see also Fig. 2 of Ref. 11, for measurements on single crystals) and remains poorly understood.

More important within the context of this paper, is that the coefficient a of the $T^{1/2}$ term is enhanced when the disorder increases (see Table I), as predicted by expression (2). Indeed, as the zero-temperature conductivity σ_0 is a measure of the degree of disorder, it is found that there is a clear correlation between the increasing relevance of quantum suppression of conductivity at low temperature and disorder. This is illustrated in Fig. 6(a), where we plot a vs σ_0 (closed symbols).

From Eqs. (1) and (2) it follows that

$$a = \lambda_F^4 \left(\frac{ne^2}{h} \right)^{3/2} \frac{(2m^* k_B)^{1/2}}{h} \sigma_0^{-1/2}. \quad (5)$$

Therefore a linear dependence of a vs $\sigma_0^{-1/2}$ is expected. As illustrated by Fig. 6(b) (closed symbols), this is just the observed behavior. Data analysis can be cross checked by evaluating the Fermi wavelength from the measured slope in Fig. 6(b). We find $\lambda_F \approx 2 \text{ \AA}$, which is in good agreement with estimates given above.

It could be argued that a 3D limit could not be appropriate to describe the physics of nanometric thin films (recall that the thickness of the films under discussion is of about 6–8 nm). We shall not discuss here which description is most appropriate, but we will emphasize that in a 2D weak-localization model, the low-temperature quantum corrections to the conductivity are described by^{28–30}

FIG. 6. The coefficient a of the quantum correction $T^{1/2}$ term is plotted against the residual conductivity σ_0 (left) and versus $\sigma_0^{-1/2}$ (right). Solid symbols correspond to ρ_{\parallel} and ρ_{\perp} of the 8 nm thick film (series A) and of the $t=6$ nm film (series B) fully described in the text. Open symbols correspond to measurements performed on two additional $t=6$ nm thin films grown on vicinal (Δ) and on exact (\circ) SrTiO₃ substrates.

$$\sigma = \sigma_0 + a' \ln T + bT^2. \quad (6)$$

If use is made of Eq. (6) to describe the experimental data, good fits can also be obtained. The important message however, is that also in this framework, the coefficient a' still displays a close relationship with the degree of disorder. Therefore the same conclusions can be drawn; i.e., quantum interference effects are *always* enhanced as disorder increases; no matter the model is used to analyze the data. Quantum corrections from electron-electron interactions are at the origin of the resistivity minima commonly observed in SRO thin films.

V. RESULTS III: FERROMAGNETIC TRANSITION

Finally we address the key issue of the magnetic transition and its dependence on thickness and, thus, the influence of disorder. In bulk SrRuO₃ specimens, the Curie temperature is T_C ($\approx 160 \text{ K}$), and the magnetic transition is charac-

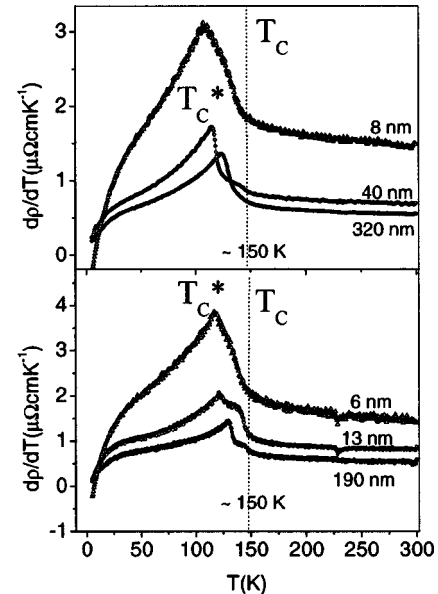


FIG. 7. The paramagnetic to ferromagnetic phase transition can be probed by plotting the $d\rho/dT$ curves against the temperature. The onset of ferromagnetism (T_C) is seen to be at $\sim 150 \text{ K}$ for all the samples (indicated by a vertical dotted line). Nevertheless, as the thickness decreases, a shift to lower temperatures is seen for the peak (T_C^*), together with a broadening of the transition, both in series A (top panel) and B (bottom panel).

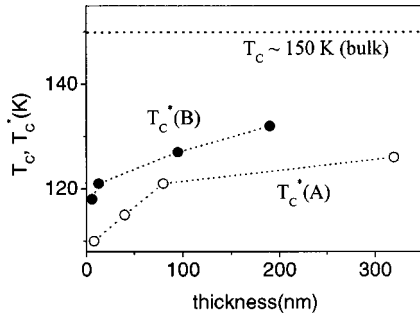


FIG. 8. The variation of T_C^* with thickness is plotted for series A [$T_C^*(A)$] and series B [$T_C^*(B)$].

terized by a peak in the derivative $d\rho/dT$ at T_C^* .²⁰ In our films, we observe (see Fig. 7) that the onset of ferromagnetic correlations—signalled by the rising of $d\rho/dT$ —remains nearly constant at ~ 150 K and that T_C^* (see Fig. 8) is progressively shifted towards a lower temperature as the thickness decreases: $T_C^* \sim (127-110)$ K for films of series A, whereas for films of series B T_C^* is somewhat higher: $\sim (132-118)$ K. Two conclusions are evident from the experimental data: (i) for all films we found that the measured T_C^* is substantially lower than the bulk value and (ii) T_C^* depends on thickness^{22,23} while T_C does not.

It is well known that the Curie temperature of SrRuO_3 decreases under hydrostatic pressures,³¹ as a result of the induced modification of the overlapping of the Ru $4d$ and O $2p$ orbitals. In the present case, however, we must stress that the films have identical in-plane cell parameters, so the substantial shift of T_C^* towards lower values as thickness decreases cannot be explained by an alteration of the cell parameters but likely it is related to the microstructural disorder concomitant to the island growth process observed at early stages of film growth. As mentioned above, the magnetic properties of the ruthenates are strongly sensitive to small distortions of the unit cell, consisting of tilts and rotations of the RuO_6 octahedra.⁸ Consequently, the hypothetical stabilization of a distinct polymorphic SrRuO_3 phase near the grain edges may lead to a local weakening of the ferromagnetic coupling whereas the rest of the system is relatively unaffected. Interestingly enough is to point out that the onset of ferromagnetism, as indicated in Fig. 7, appears in all films at $T \approx 150$ K, so that there are always regions relatively undistorted where the ferromagnetic correlations appear at this temperature, and these regions are more significant as the thickness increases, i.e., when disorder decreases. When the thickness decreases the broadening of the $d\rho/dT$ curve reflects the broadening of the transition and a decrease of T_C^* results.

VI. CONCLUSIONS

The evolution of the magnetotransport properties in nanometric epitaxial SrRuO_3 thin films grown on SrTiO_3 sub-

strates has been analyzed. 3D growth occurs at the first stages, eventually evolving to a 2D step flow growth. The initial growth leads to the formation of finger-shaped 3D elongated growth islands aligned to the substrate steps that coalesce at a critical thickness of t around 10 nm. This peculiar behavior leads to a dramatic in-plane anisotropy of the resistivity, even in films with a very regular surface. We argue that the presence of defective regions, occurring where the growth islands merge, is at the origin of the observed anisotropy. We suggest that the existence of the complex phase transformation in SrRuO_3 upon cooling is at the origin of these remarkable transport properties. In addition, we have presented experimental procedures to reduce these defects. The presence of microstructural disorder leads also to a reduction of the residual conductivity and thus the mean free path of carriers shrinks. We have shown that this promotes a reinforcement of the electron-electron correlations that can be understood on the framework of current ideas of effects of disorder in strongly correlated electronic systems. Accordingly, we have shown that the electron-electron correlations clearly correlate with the degree of disorder and thus they become prominent in nanometric thin films. Finally, the broadening and shift towards lower temperatures of the kink in the resistivity curves (that signals the Curie temperature) are also found to be intimately related with disorder and are more relevant when film thickness is reduced. In spite of this, the onset of ferromagnetic correlations remains fixed at a constant temperature.

The results reported here illustrate the extreme sensitivity of strongly correlated systems to disorder and thus to the initial stages of film growth. The fact that the mean free path l is close to the electronic Fermi wavelength λ_F is at the origin of the enhancement of quantum corrections at low temperature. Given that SrRuO_3 is an attractive oxide being used already in some applications and being considered as a candidate for technological developments, the present findings may have a deep relevance in the fabrication of multilayered technological devices, such as magnetic tunneling or ferroelectric junctions and to overcome the difficulties pointed out above.

After submission of this paper, we have performed some further measurements that reinforce the main lines here outlined. According to the experimental work of other authors, the vicinity of the SrTiO_3 substrates has a strong influence on the growth of SrRuO_3 thin films.^{16,27} In agreement with these findings, we are able to control the degree of microstructural disorder of the SrRuO_3 thin films by growing them on miscut SrTiO_3 substrates. We have grown two films with $t = 6$ nm in the same conditions but on different substrates, one with a nominal zero-miscut angle, and the other with a miscut angle of 2° .³² The experimental results reveal the expected behavior, i.e., the film grown on the vicinal substrate has a lower degree of disorder as indicated by the lower temperature at which the resistivity minima appear. Indeed, for this film, no resistivity minimum is observed at $T \geq 5$ K when current is injected along the substrate steps. Therefore,

this procedure has allowed us to add three new points to Figs. 6(a) and 6(b), marked as open circle symbols. We observe that these new points follow the trend found in the previous experiments (closed circle symbols), i.e., they follow the same a vs $\sigma_0^{-1/2}$ and a vs σ_0 laws as the previous ones, and this fact corroborates the findings showed in the present paper.

ACKNOWLEDGMENTS

We acknowledge financial support from the MCyT (Spain) Project Nos. MAT99-0984-CO3, MAT2000-1290-CO3-03, and MAT2002-04551-CO3. We are thankful to Dr. Luis Brey for fruitful discussions, and to Professor Domingo González for his support.

*Electronic address: gherranz@icmab.es

†Present address: Institut de Ciència de Materials de Barcelona, CSIC, Campus UAB, Bellaterra 08193, Catalunya, Spain.

- ¹R. M. Stroud, A. T. Hanbicki, Y. D. Park, G. Kioseoglou, A. G. Petukhov, B. T. Jonker, G. Itskos, and A. Petrou, *Phys. Rev. Lett.* **89**, 166602 (2002).
- ²M. Bibes, LL. Balcells, S. Valencia, J. Fontcuberta, M. Wojcik, E. Jedryka, and S. Nadolski, *Phys. Rev. Lett.* **87**, 067210 (2001).
- ³C. B. Eom, R. J. Cava, R. M. Fleming, J. M. Philips, R. B. van Dover, J. H. Marshall, J. W. P. Hsu, J. J. Krajewski, and W. F. Peck, *Science* (Washington, DC, U.S.) **258**, 1766 (1992).
- ⁴P. B. Allen, H. Berger, O. Chauvet, L. Forro, T. Jarlborg, A. Junod, B. Revaz, and G. Santi, *Phys. Rev. B* **53**, 4393 (1996).
- ⁵I. Mazin and D. J. Singh, *Phys. Rev. B* **56**, 2556 (1997).
- ⁶T. Kiyama, K. Yoshimura, K. Kosuge, H. Mitamura, and T. Goto, *J. Phys. Soc. Jpn.* **68**, 3372 (1999).
- ⁷M. Bibes, B. Martínez, J. Fontcuberta, V. Trtik, F. Benítez, C. Ferrater, F. Sánchez, and M. Varela, *Phys. Rev. B* **60**, 9579 (1999).
- ⁸G. Cao, S. McCall, M. Shepard, J. E. Crow, and R. P. Guertin, *Phys. Rev. B* **56**, 321 (1997).
- ⁹M. A. López de la Torre, Z. Sefrioui, D. Arias, M. Varela, J. E. Villegas, C. Ballesteros, C. León, and J. Santamaría, *Phys. Rev. B* **63**, 052403 (2001).
- ¹⁰J. Okamoto, T. Mizokawa, A. Fujimori, I. Hase, M. Nohara, H. Takagi, Y. Takeda, and M. Takano, *Phys. Rev. B* **60**, 2281 (1999).
- ¹¹L. Capogna, A. P. Mackenzie, R. S. Perry, S. A. Grigera, L. M. Galvin, P. Raychaudhuri, A. J. Schofield, C. S. Alexander, G. Cao, S. R. Julian, and Y. Maeno, *Phys. Rev. Lett.* **88**, 076602 (2002).
- ¹²M. Izumi, K. Nakazawa, and Y. Bando, *J. Phys. Soc. Jpn.* **67**, 651 (1997).
- ¹³M. Izumi, K. Nakazawa, Y. Bando, Y. Yoneda, and H. Terauchi, *Solid State Ionics* **108**, 227 (1998).
- ¹⁴J. Choi, C. B. Eom, G. Rijnders, H. Rogalla, and D. H. A. Blank, *Appl. Phys. Lett.* **79**, 1447 (2001).
- ¹⁵Q. Gan, R. A. Rao, C. B. Eom, J. M. Garrett, and M. Lee, *Appl. Phys. Lett.* **72**, 978 (1998).
- ¹⁶D. B. Kacedon, R. A. Rao, and C. B. Eom, *Appl. Phys. Lett.* **71**, 1724 (1997).
- ¹⁷D. B. Zakharov, K. M. Satyalakshmi, G. Koren, and D. Hesse, *J. Mater. Res.* **14**, 4385 (1999).
- ¹⁸C. L. Chen, Y. Cao, Z. J. Huang, Q. D. Jiang, Z. Zhang, Y. Y. Sun, W. N. Kang, L. M. Dezaneti, W. K. Chu, and C. W. Chu, *Appl. Phys. Lett.* **71**, 1047 (1997).
- ¹⁹J. H. Cho, Q. X. Jia, X. D. Wu, S. R. Foltyn, and P. Maley, *Phys. Rev. B* **54**, 37 (1996).
- ²⁰L. Klein, J. S. Dodge, C. H. Ahn, G. J. Snyder, T. H. Geballe, M. R. Beasley, and A. Kapitulnik, *Phys. Rev. Lett.* **77**, 2774 (1996).
- ²¹R. H. Chae, R. A. Rao, and C. B. Eom, *J. Electroceram.* **4**, 345 (2000).
- ²²G. Herranz, F. Sánchez, M. V. García-Cuenca, C. Ferrater, M. Varela, B. Martínez, and J. Fontcuberta, *Appl. Phys. Lett.* **82**, 85 (2003).
- ²³G. Herranz, F. Sánchez, M. V. García-Cuenca, C. Ferrater, M. Varela, B. Martínez, and J. Fontcuberta, in *Spintronics*, edited by T. J. Klemmer, J. Z. Sun, A. Fert, and J. Bass, MRS Symposia Proceedings No. 690 (Materials Research Society, Warrendale, PA, 2002), p. 43.
- ²⁴F. Sánchez, M. V. García-Cuenca, C. Ferrater, M. Varela, G. Herranz, B. Martínez, and J. Fontcuberta (unpublished).
- ²⁵B. J. Kennedy, B. A. Hunter, and J. R. Hester, *Phys. Rev. B* **65**, 224103 (2002).
- ²⁶M. Shepard, S. McCall, G. Cao, and J. E. Crow, *J. Appl. Phys.* **81**, 4978 (1997).
- ²⁷L. Klein, J. S. Dodge, C. H. Ahn, J. W. Reiner, L. Mieville, T. H. Geballe, M. R. Beasley, and A. Kapitulnik, *J. Phys.: Condens. Matter* **8**, 10 111 (1996).
- ²⁸P. A. Lee and T. V. Ramakrishnan, *Rev. Mod. Phys.* **57**, 287 (1985).
- ²⁹B. L. Altshuler and A. G. Aronov, *Electron-Electron Interaction in Disordered Conductors*, edited by A. L. Efros and M. Pollak (North-Holland, Amsterdam, 1985).
- ³⁰*Fundamentals of the Theory of Metals*, edited by A. Abrikosov (North-Holland, Amsterdam, 1988).
- ³¹F. Le Marrec, A. Demuer, D. Jaccard, J.-M. Triscone, M. K. Lee, and C. B. Eom, *Appl. Phys. Lett.* **80**, 2338 (2002).
- ³²G. Herranz, F. Sánchez, M. V. García-Cuenca, C. Ferrater, M. Varela, B. Martínez, and J. Fontcuberta (unpublished).